

1 **Influenza A virus reassortment in mammals gives rise to genetically distinct within-host sub-
2 populations**

3
4 Ketaki Ganti¹, Anish Bagga², Silvia Carnaccini³, Lucas M. Ferreri^{1,3}, Ginger Geiger³, C. Joaquin
5 Caceres³, Brittany Seibert³, Yonghai Li⁴, Liping Wang⁵, Taeyong Kwon⁴, Yuhao Li⁴, Igor Morozov⁴,
6 Wenjun Ma^{5,6}, Juergen A. Richt^{4,6}, Daniel R. Perez^{3,7}, Katia Koelle^{8,9} and Anice C. Lowen^{1,9}

7
8 ¹Department of Microbiology and Immunology, Emory University School of Medicine, Atlanta,
9 GA, USA

10 ²Emory College of Arts and Sciences, Atlanta, GA, USA

11 ³Department of Population Health, College of Veterinary Medicine, University of Georgia,
12 Athens, GA, USA

13 ⁴Department of Diagnostic Medicine and Pathobiology, College of Veterinary Medicine, Kansas
14 State University, Manhattan, KS, USA

15 ⁵Department of Veterinary Pathobiology, and Department of Molecular Microbiology and
16 Immunology, University of Missouri, Columbia, MO, USA

17 ⁶St Jude Center of Excellence for Influenza Research and Response (SJ-CEIRR)

18 ⁷The Center for Research on Influenza Pathogenesis and Transmission (CRIP CEIRR)

19 ⁸Department of Biology, Emory University, Atlanta, GA

20 ⁹Emory Center of Excellence for Influenza Research and Response (Emory-CEIRR)

21
22 **Abstract**
23 Influenza A virus (IAV) genetic exchange through reassortment has the potential to accelerate
24 viral evolution and has played a critical role in the generation of multiple pandemic strains. For
25 reassortment to occur, distinct viruses must co-infect the same cell. The spatio-temporal
26 dynamics of viral dissemination within an infected host therefore define opportunity for
27 reassortment. Here, we used wild type and synonymously barcoded variant viruses of a pandemic
28 H1N1 strain to examine the within-host viral dynamics that govern reassortment in guinea pigs,
29 ferrets and swine. The first two species are well-established models of human influenza, while

30 swine are a natural host and a frequent conduit for cross-species transmission and reassortment.
31 Our results show reassortment to be pervasive in all three hosts but less frequent in swine than
32 in ferrets and guinea pigs. In ferrets, tissue-specific differences in the opportunity for
33 reassortment are also evident, with more reassortants detected in the nasal tract than the lower
34 respiratory tract. While temporal trends in viral diversity are limited, spatial patterns are clear,
35 with heterogeneity in the viral genotypes detected at distinct anatomical sites revealing
36 extensive compartmentalization of reassortment and replication. Our data indicate that the
37 dynamics of viral replication in mammals allow diversification through reassortment but that the
38 spatial compartmentalization of variants likely shapes their evolution and onward transmission.

39

40 **Introduction**

41 Influenza A viruses (IAVs) have a broad host range, with the greatest diversity in wild bird species
42 and established lineages circulating in poultry, swine, humans and other mammalian hosts^{1,2}.
43 Host range for a given lineage is restricted by species barriers to infection, but occasional spillover
44 events can result in sustained transmission, seeding new lineages^{3,4}. Establishment of novel IAVs
45 in humans is the source of influenza pandemics and has major ramifications for public health and
46 the economy^{5,6}. Reassortment of gene segments between IAVs adapted to distinct host species
47 can give rise to chimeric viruses with enhanced potential for cross-species transfer⁷. Prominent
48 examples include the reassortant strains that gave rise to the 1957, 1968 and 2009 influenza
49 pandemics^{8,9}.

50 Among non-human mammalian species, swine are of particular interest. Transmission of IAV
51 between swine and humans is relatively common, due not only to an extensive interface in
52 agricultural settings, but also to similarities between pigs and humans in the host factors that
53 support viral replication^{10,11}. Swine hosts are also somewhat susceptible to infection with avian
54 IAV, creating the opportunity for co-infection and reassortment of viruses that are typically
55 separated by host species barriers¹². For this reason, swine are often referred to as mixing vessels
56 for IAV reassortment^{13,14}. The role of swine in the 2009 influenza pandemic⁹, and the abundant
57 reassortment that characterizes IAV in swine¹⁵⁻¹⁹, offer ample support for this designation.

58 Although the central position of swine in IAV ecology and evolution is well understood^{10,13,16}, the
59 within-host viral dynamics that govern reassortment in this host are less well characterized.
60 We have previously reported that IAV reassortment occurs frequently *in vivo*²⁰⁻²⁴. This prior work
61 focused on easily sampled IAV populations replicating in the upper respiratory tracts of
62 mammals. Recent work has shown, however, that distinct within-host subpopulations can form
63 in different regions of the respiratory tract²⁵. This spatial structure, in turn, can influence viral
64 evolutionary dynamics within and between hosts^{26,27}. Here, we evaluated how genotypic
65 diversity generated through reassortment is shaped by and contributes to viral population
66 structure within the host.

67 We examined within-host diversity generated through reassortment in guinea pigs, ferrets and
68 pigs. While pigs are an important natural host, guinea pigs and ferrets are well-characterized
69 models for human IAV²⁸⁻³⁰. We find that co-infection at the cellular level is extensive and
70 reassortant viruses are consistently observed. In ferrets, markedly greater viral genotypic
71 diversity is generated in the upper respiratory tract compared to the lower tract. Viral
72 populations at these two sites are furthermore highly dissimilar genetically, revealing strong
73 spatial compartmentalization. Diversity generated through reassortment in swine is generally
74 lower than in guinea pigs and ferrets and, as in ferrets, viral diversity in swine is characterized by
75 extensive spatial compartmentalization. Taken together, our data reveal spatial structure within
76 the mammalian respiratory tract to be a major factor defining the extent of IAV diversity
77 engendered through reassortment.

78

79 **Results**

80 **Viral genotypic diversity generated through reassortment in the mammalian nasal tract**

81 To evaluate the viral genotypic diversity generated via reassortment, guinea pigs, ferrets and pigs
82 were coinfecte with well-matched parental viruses of the influenza A/Netherlands/602/2009
83 (NL09; pH1N1) background³¹. Termed wild type (WT) and variant (VAR), these coinfecting viruses
84 differ by a single synonymous mutation introduced into each gene segment of the VAR virus and
85 distinct epitope tags encoded in the hemagglutinin open reading frame of each virus. In cell
86 culture, these two viruses show comparable fitness (Supplementary Fig. 1). Following

87 determination of the 50% infectious dose (ID_{50}) of the virus mixture in ferrets and utilizing prior
88 ID_{50} results in guinea pigs³², reassortment in these species was analyzed at two doses applied
89 intranasally (1×10^2 and $1 \times 10^5 ID_{50}$). In pigs, a single dose of 2×10^6 PFU applied both intranasally
90 and intratracheally was used after preliminary tests with lower, intranasal, doses showed that
91 animals were not consistently infected. All inoculated animals supported robust viral replication,
92 as assessed at the nasal site, with titers declining to the limit of detection by day 4-7 post-
93 inoculation (Supplementary Fig. 2).

94 To monitor reassortment in the upper respiratory tract, nasal samples were collected
95 longitudinally, and the genotypes of clonal isolates derived from each sample were determined.
96 The parental origin of each of the eight segments was defined, allowing identification of all 254
97 possible reassortant genotypes and both parental genotypes. Here, a genotype is defined as a
98 constellation of eight gene segments and any nucleotide diversity present is not considered.
99 Reassortment was detected in all samples from all species tested (Supplementary Fig. 3). To
100 characterize the viral diversity generated through reassortment, we calculated the frequency of
101 unique genotypes, frequency of parental genotypes, richness, and Shannon-Weiner diversity for
102 each sample (Fig. 1).

103 In all three host species, the same reassortant virus is rarely detected across multiple time points
104 (Supplementary Fig. 3), suggesting genotypic loss due to stochastic processes such as drift or
105 disruption through further reassortment. Parental genotypes (WT or VAR), however, are
106 consistently detected in the nasal samples of each animal in least two time points (Fig. 1B, F, J,
107 M). Despite efforts to inoculate with a 1:1 mixture of WT and VAR viruses, VAR was predominant;
108 this could reflect a skewing in the inoculum or fitness advantage of VAR that is only apparent *in*
109 *vivo*. Since 21 viral isolates were genotyped from each sample, richness has a maximum value of
110 21 in our dataset. Richness is often high in guinea pigs and ferrets, with values ranging from 4 to
111 18, while the range in pigs falls between 3 and 10 (Fig. 1C, G, K, N). Trends in diversity correspond
112 to those of richness (Fig. 1D, H, L, O).

113 In guinea pigs and ferrets, only marginal effects of dose were apparent (Fig. 1, compare dashed
114 and solid lines). Nevertheless, as shown in Supplementary Fig. 4, differences in diversity across
115 doses were significant in both species, with the higher dose yielding higher diversity when all

116 time points were considered together ($p=0.04$ in guinea pigs and $p=0.003$ in ferrets, ANOVA).
117 Richness was also significantly higher in ferrets receiving a higher dose ($p=0.002$, ANOVA).
118 The effects of dose are relevant in interpreting comparisons across species as only a relatively
119 high dose was tested in pigs. Comparison of species across all time points and doses shows
120 significantly higher richness and diversity in guinea pigs and ferrets than in pigs (Fig. 1N, O;
121 $p<0.01$, ANOVA). Limiting this analysis to include only animals receiving a high dose of inoculum
122 confirmed these trends ($p<0.005$, ANOVA).
123 Overall, these results reveal that the mammalian upper respiratory tract presents an
124 environment with high potential for the generation of viral diversity via reassortment, with
125 modest effects of dose observed and with swine showing lower viral diversity than guinea pigs
126 or ferrets.

127
128 **Viral diversity generated through reassortment is greater in the ferret nasal tract than in the**
129 **lungs.** In mammalian hosts, IAV replication can be distributed throughout the respiratory tract.
130 Using the ferret model, we compared the extent of viral diversity arising through reassortment
131 in upper and lower respiratory tracts. Nasal turbinates and lung tissues were collected on days 1,
132 2, 3 or 4 from ferrets inoculated with 1×10^2 or 1×10^5 ferret ID₅₀. Viral titers in these samples are
133 reported in Supplementary Fig. 2. Genotyping of viral isolates revealed that the number of unique
134 genotypes detected was routinely higher in nasal turbinates compared to lung at both doses (Fig.
135 2A–C). Similarly, Shannon-Weiner diversity in nasal turbinates was typically higher than in the
136 lung (Fig. 2D). These differences in both richness and diversity were significant (Fig. 2E, F)
137 ($p=8.6\times10^{-5}$ and $p=0.0014$, respectively; paired t-test).
138 We hypothesized that the distinct outcomes of co-infection in the upper and lower respiratory
139 tracts were indicative of little viral dispersal between the two sites. To test this hypothesis, we
140 modeled free mixing between the lung and nose by computationally shuffling intact genotypes
141 between the two tissues. We then compared our observed data to the resultant simulated
142 dataset (Fig. 2C, D). This approach revealed that richness and diversity seen in the lungs is low
143 relative to that expected for free mixing, with observed values typically falling below the 5th
144 percentile of simulated results. In contrast, richness and diversity observed in nasal turbinates is

145 typically above the mean. This analysis suggests that spread of virus between upper and lower
146 respiratory locations occurs relatively rarely, such that abundant diversity generated through
147 reassortment in the nasal tract does not seed a similarly diverse population in the lungs.

148

149 **Reassortant viral populations in the ferret upper and lower respiratory tracts are distinct.**
150 Examination of the specific genotypes identified in the nasal turbinates and lung within a given
151 ferret revealed almost no overlap (Fig. 2A, B). To more rigorously assess this apparent
152 dissimilarity of viral populations, we calculated normalized beta diversity (β_n) between pairs of
153 samples³³. This dissimilarity metric has a range between 0 and 1, with a beta value of 0 indicating
154 that two samples are identical in their genotype composition, and a beta value of 1 indicating no
155 genotypic overlap. In all ferrets, high beta diversities of >0.5 are seen between nasal turbinate
156 and lung samples of the same animal (Fig. 3A). Indeed, beta diversity values calculated between
157 pairs of samples within and between ferrets indicate that the nasal and lung viral populations
158 within an individual are typically as distinct as populations replicating in different animals (Fig.
159 3A). To test whether a lack of viral dispersal between anatomical sites could account for this
160 observation, we compared the observed beta diversity to the distribution of beta diversity values
161 obtained from the computational simulation of free mixing outlined above. For most ferrets,
162 observed beta diversity falls above the 95th percentile of the distribution (Fig. 3B). Thus, the highly
163 distinct viral populations seen in nasal and lung tissues are inconsistent with free mixing between
164 these sites. These data further support the notion that virus replicating within the ferret upper
165 and lower respiratory tracts form distinct compartments, with reassortment occurring
166 independently at the two sites.

167 To visualize the spatial distribution of coinfecting viruses within ferret tissues, the tagged HA
168 proteins of WT and VAR origin were stained within lung and nasal tissue sections (Fig. 3C). This
169 analysis revealed that microscopic fields that are positive for viral antigen tend to show a high
170 density of infected cells at both tissue sites. Strikingly, most infected cells are positive for both
171 WT and VAR antigens, indicating high levels of viral co-infection within the host, consistent with
172 the robust reassortment observed. The cell types hosting viral antigen in the infected lung tissue
173 were defined based on their morphology and found to comprise ciliated epithelium of the

174 bronchi and bronchioles, goblet cells, cells of the peribronchial/-iolar submucosal glands and type
175 II pneumocytes within the alveoli (Fig. 3D and Supplementary Table 2). Unfortunately, this
176 analysis could not be performed for nasal turbinate owing to exhaustion of the samples.

177

178 **Local diversity arising through reassortment is modest within the swine respiratory tract.**

179 Analysis of nasal swabs showed limited genotypic diversity in the swine nasal tract. We expanded
180 this investigation of reassortment in pigs by sampling the nasal tract and each of the seven lung
181 lobes of groups of three pigs on day 3 or 5 post-inoculation. Viral titers in these samples are
182 shown in Supplementary Fig. 2. Titers in the nasal tract on day 3 were insufficient to support
183 analysis of reassortment. Genotype frequencies observed from the remaining sites were plotted
184 and overlaid on a schematic of a pig lung (Fig. 4A-F). Although one or more reassortants are
185 detected in all but three of the 45 samples, the viral populations tend to carry high proportions
186 of parental virus. At a minority of sites, a specific reassortant is predominant. Richness is less than
187 10 for most samples (Fig. 4G) and Shannon-Weiner diversities less than 1.0 are common (Fig. 4H).
188 Thus, overall, the diversity generated through reassortment throughout the swine respiratory
189 tract is moderate. To evaluate the extent to which a lack of viral mixing across the sampled
190 locations limits richness and diversity, we compared the observed results to those expected if
191 viruses mix freely throughout the respiratory tract (Fig. 4G, H). To simulate free mixing, we
192 randomly sampled intact viral genotypes from all those detected within a given pig. The resultant
193 richness and Shannon-Weiner diversity values show wide distributions. However, much of the
194 observed data lies below the 5th percentile of these distributions, suggesting that pockets of low
195 richness and diversity persist locally due to an absence of mixing across anatomical sites. In sum,
196 local genotypic diversity generated via reassortment is modest throughout the swine respiratory
197 tract.

198

199 **Reassortant viral populations show extensive compartmentalization within the swine**
200 **respiratory tract.** Examination of the reassortant viral genotypes identified in swine tissues
201 reveals little to no overlap across locations within an individual animal (Fig. 4A-F). We again used
202 beta diversity to assess the similarity of viral populations in a pairwise and quantitative manner.

203 As seen in ferrets, beta values in pigs were typically high (Fig. 5A and Supplementary Fig. 5).
204 Indeed, viral populations sampled from within a pig were as distinct from one another as those
205 sampled from different pigs (Fig. 5A). To test whether a lack of viral dispersal between anatomical
206 sites could account for this observation, we compared the beta diversity observed for a pair of
207 locations within a pig to the distribution of beta diversity values obtained from a simulation of
208 free mixing between those locations (Fig. 5B and Supplementary Fig. 6). For most pairs of tissues,
209 the observed data are at the high extreme of this distribution, falling within the 95th percentile
210 of the simulated results. Thus, spatial compartmentalization within the swine respiratory tract is
211 extensive.

212 To visualize the spatial distribution of co-infecting viruses within swine tissues, the tagged HA
213 proteins of WT and VAR origin were stained (Fig. 5C and Supplementary Fig. 7). As in ferrets, a
214 high density of infected cells is visible in regions positive for viral antigen and most infected cells
215 are positive for both WT and VAR viruses. Thus, the high levels of viral co-infection observed in
216 ferrets extends to swine. Using a morphologic approach to identify cell types, we found type II
217 pneumocytes within the alveoli and ciliated epithelial cells of the bronchioles and bronchi to be
218 the predominant cell types harboring viral antigen in the lungs (Fig. 5D, Supplementary Fig. 8 and
219 Supplementary Table 2). In nasal turbinates, viral antigen positivity was observed within
220 respiratory and transitional epithelia (Supplementary Fig. 8 and Supplementary Table 2).

221

222 **Discussion**

223 Our experiments reveal the extent to which co-infection at the level of the whole host creates
224 opportunity for reassortment within the host. Abundant opportunity is apparent in the nasal
225 tracts of guinea pigs and ferrets. However, the viral diversity generated through reassortment is
226 more limited in the lungs of ferrets and all tissues sampled in pigs. In addition to relatively little
227 opportunity for reassortment in these tissues, spatial constraints on mixing within the respiratory
228 tract yield localized sub-populations with diminished genotypic diversity. Thus, despite the
229 extensive reassortment seen among swine IAV at a population level, our results reveal only
230 moderate viral diversity generated through reassortment in pigs. Results from guinea pigs and

231 ferrets suggest that opportunity for within-host IAV genetic exchange may be greater in other
232 natural mammalian hosts.

233 In drawing comparisons across the species examined, it is important to consider differences in
234 the protocols applied. Swine were infected both intranasally and intratracheally compared to
235 only intranasal infection in both ferrets and guinea pigs. The delivery of inoculum directly to the
236 lower respiratory tract in swine might be expected to augment potential for WT-VAR coinfection
237 in the lungs. In addition, swine were infected with a single high dose with unknown relationship
238 to the median infectious doses in this species, while ferrets and guinea pigs were each infected
239 with doses of 1×10^2 and 1×10^5 ID₅₀. As measured by plaque assay, the dose applied in pigs is
240 comparable to the high dose used in guinea pigs and approximately 10-fold lower than the high
241 dose used in ferrets. While inoculum dose might be expected to influence the potential for
242 coinfection and propagation of novel variants, the effect of a 10³-fold difference in dose in ferrets
243 and guinea pigs was modest. We therefore suggest that the more limited diversification through
244 reassortment in pigs is unlikely to be due to protocol differences.

245 Given our use of well-matched parental viruses, the differences in viral genotypic diversity seen
246 between species and between tissues within a species are also unlikely to be driven by selection.
247 Instead, features of viral dynamics in these different environments likely shape the frequency of
248 reassortment and the extent to which reassortants are amplified once formed. Since relatively
249 few reassortants were detected in pigs and in ferret lungs, our data imply that the size of the
250 target tissue may be an important factor. In a large animal such as swine or a tissue with extensive
251 surface area, such as lung, the likelihood of cellular co-infection involving genetically distinct
252 variants may be reduced. In addition, viral fitness, the spatial arrangement of target cells, the
253 extent to which permissive cells are interspersed with non-permissive cells, physical barriers to
254 viral spread and the effectiveness innate responses to infection are all likely to vary with species
255 and across different tissues within a species³⁴⁻³⁶.

256 Although variation in the diversity generated through reassortment is apparent, visualization of
257 viral antigen in infected tissues indicated that cellular co-infection is abundant at all sites
258 examined. Cellular co-infection has previously been reported to be common *in vivo*³⁷ and is
259 expected owing to the high potential for singular genomes to result in abortive infection^{38,39} and

260 the potential for direct cell-to-cell spread of viral genetic material⁴⁰. Nevertheless, the
261 juxtaposition of this result with a predominance of parental-type viruses in many samples is
262 counter-intuitive. While the images of fixed tissue show a snapshot of viral HA protein expression
263 in defined cells at a given time point, viral samples draw from the population of viruses that have
264 accumulated at a particular site over the course of infection. Thus, the prevalence of parental
265 genotypes may reflect their production early after inoculation, when cellular co-infection is less
266 likely to occur^{22,37}. In addition, HA staining does not reveal the relative dosage of WT and VAR
267 genomes in a cell or indicate the genotype(s) of the seven non-HA segments. Both factors would
268 strongly modulate the proportion of progeny genomes from a co-infected cell that are
269 reassortant.

270 The spatial separation of viral sub-populations within an individual has important evolutionary
271 implications. First, reassortment among genetically distinct viruses is less likely to occur when
272 viral dispersal is localized, since all viruses produced from a singly infected progenitor cell will be
273 genetically similar²³. Conversely, well-mixed viral populations are more likely to produce
274 reassortants that differ from their parents in biologically meaningful ways. Compartmentalization
275 of variants may be a contributing factor to the lack of reassortment reported in experimentally
276 infected humans⁴¹. Second, spatial structure impacts the extent to which a viral population within
277 a host is shaped by selection versus stochastic processes^{25,42}. Spatial barriers create
278 subpopulations, each of which can have a small population size. As such, genetic drift dominates
279 within each subpopulation, with variant frequencies changing over time largely due to chance.
280 This means that both lower and higher fitness variants have the potential to rise to high
281 frequencies within subpopulations. As a result, spatial compartmentalization of populations has
282 the immediate effect of reducing the efficiency of selection. While the strength of selection to
283 purge low fitness variants is weakened at the level of individual subpopulations, the propagation
284 of slightly deleterious mutants allows a broader exploration of sequence space across the entire
285 viral population that is distributed within the host. This may, in rare cases, lead to the discovery
286 of higher fitness variants that might not evolve as readily in less structured within-host
287 populations.

288 Compartmentalization of viral replication is also expected to shape evolution occurring between
289 hosts. As has been seen in ferrets, transmitted virus is likely to comprise a sub-sample of one
290 specific anatomical location^{23,27,43}. In the context of spatial heterogeneity, this sub-sample will
291 not be representative of the viral population present in the whole host. Thus, within-host spatial
292 structure is expected to contribute to stochastic effects acting between hosts: the transmitted
293 virus will be the virus that was in the right place at the right time, and may not be the most fit
294 genotype present within a host^{23,27,44,45}.

295 Certain limitations in our experimental design are important to consider. Our approach of co-
296 inoculating with well-matched parental strains is designed to maximize potential to detect
297 reassortment. In addition, the gene constellation of the 2009 pandemic H1N1 virus, used in this
298 study, has shown a marked predisposition for reassortment⁴⁶⁻⁴⁸. However, natural co-infections
299 will include a wide range of scenarios in terms of relative timing, route and dose of infection and
300 phenotypes of co-infecting strains. Each of these factors will influence the frequency of
301 reassortment^{21-23,49}. In evaluating the extent of overlap between viral genotypes in different
302 anatomical locations, it is important to note that parental viruses are likely seeded throughout
303 the respiratory tract upon inoculation; thus, only reassortant genotypes are informative in
304 assessing the extent of mixing across sites. In addition, if variants are rare (<5%), they would fall
305 below the limit of detection of our assay, which can have potent effects on measured beta
306 diversity. In particular, if a genotype detected in one location is present below the limit of
307 detection in a second location, measured beta diversity would not reflect this commonality and
308 would therefore be erroneously high.

309 IAV reassortment within cells is efficient, such that 256 distinct genotypes are readily formed in
310 a single co-infected cell⁵⁰. However, within a host, the high potential for reassortment to
311 generate diversity is subject to complex dynamics that define the likelihood of cellular co-
312 infection and the extent to which novel reassortants are propagated. While our data reveal
313 extensive co-infection *in vivo* and consistent formation of reassortants, species and tissue
314 differences in the extent of reassortment are apparent. Spatial constraints on the dissemination
315 of novel genotypes add to this complexity and are likely to be a major factor in within-host viral
316 evolutionary dynamics.

317 **Author Contributions**

318 KG contributed to the conception of work, experimental design, data acquisition and analysis,
319 interpretation of data; AB contributed to data analysis, model development and interpretation
320 of data; SC contributed to experimental design, data acquisition and interpretation of data; LMF,
321 GG, CJC, BS, YL, LW, TK, YL and IM contributed to data acquisition; WM, JAR and DRP contributed
322 to conception of the work, experimental design, data analysis and interpretation; KK contributed
323 to conception of the work, data analysis and interpretation; ACL contributed to conception of
324 work, experimental design and data analysis and interpretation. All authors contributed to the
325 writing of the manuscript.

326

327 **Conflict of interest statement**

328 The JAR laboratory received support from Tonix Pharmaceuticals, Xing Technologies and Zoetis,
329 outside of the reported work. JAR is inventor on patents and patent applications on the use of
330 antivirals and vaccines for the treatment and prevention of virus infections, owned by Kansas
331 State University, KS.

332

333 **Methods**

334 **Cells and cell culture media.** Madin–Darby canine kidney (MDCK) cells, a gift from Dr. Robert
335 Webster, St Jude Children’s Research Hospital, Memphis, TN to D.R.P were used for all
336 experiments. A seed stock of MDCK cells at passage 23 was subsequently amplified and
337 maintained in Minimal Essential Medium (Gibco) supplemented with 10% fetal bovine serum
338 (FBS; Atlanta Biologicals) and Normocin (Invivogen). 293T cells (ATCC, CRL-3216) were
339 maintained in Dulbecco’s Minimal Essential Medium (Gibco) supplemented with 10% FBS and PS.
340 All cells were cultured at 37°C and 5% CO₂ in a humidified incubator. The cell lines were not
341 authenticated. All cell lines were tested monthly for mycoplasma contamination while in use. The
342 medium for the culture of IAV in MDCK cells (virus medium) was prepared by supplementing the
343 basal medium for the relevant cell type with 4.3% BSA and Normocin.

344

345 **Viruses.** Viruses used in this study were derived from influenza A/Netherlands/602/2009 (H1N1)
346 virus (NL09) and were generated by reverse genetics⁵¹⁻⁵³. In brief, 293T cells transfected with
347 reverse-genetics plasmids 16–24 h previously were co-cultured with MDCK cells at 37°C for 40–
348 48 h. Recovered virus was propagated in MDCK cells at a low multiplicity of infection to generate
349 working stocks. Titration of stocks and experimental samples was carried out by plaque assay in
350 MDCK cells. Silent mutations were introduced into each segment of the VAR virus by site-directed
351 mutagenesis of reverse genetics plasmids. The specific changes introduced into the VAR virus
352 were reported previously^{24,31}. NL09 VAR virus was engineered to contain a 6XHIS epitope tag plus
353 a GGGS linker at the amino (N) terminus of the HA protein following the signal peptide. NL09 WT
354 virus carries an HA epitope tag plus a GGGS linker inserted at the N terminus of the HA protein³¹.
355 For animal challenges, 1:1 mixture of NL09 WT and VAR viruses was prepared using methods
356 described previously²⁴. This mixture was validated in cell culture by quantifying cells positive for
357 HIS and HA tags following infection of MDCK cells, revealing an empirically determined ratio of
358 0.95:1 (WT:VAR). The same mixture was used for all experiments reported herein.

359

360 **Evaluation of viral replication in cell culture.** Replication of NL09, NL09 WT and NL09 VAR viruses
361 was determined in triplicate culture wells. MDCK cells in 6 well dishes were inoculated at an MOI
362 of 0.05 PFU/cell in PBS. After 1 h incubation at 37°C, inoculum was removed, cells were washed
363 3x with PBS, 2 mL virus medium was added to cells and dishes were returned to 37 °C. A 120 ul
364 volume of culture medium was sampled at the indicated times points and stored at -80°C. Viral
365 titers were determined by plaque assay on MDCK cells.

366

367 **Animal models and reassortment *in vivo*.** All the animal experiments were conducted in
368 accordance with the Guide for the Care and Use of Laboratory Animals of the National Institutes
369 of Health. The studies were conducted under animal biosafety level 2 containment and approved
370 by the IACUC of Emory University (DAR-2002738-ELMNTS-A) for guinea pig (*Cavia porcellus*), the
371 IACUC of the University of Georgia (AUP A2015 06-026-Y3-A5) for ferret (*Mustela putorius furo*)
372 and the IACUC of Kansas State University (protocol #4120) for swine (*Sus scrofa*). The animals

373 were humanely euthanized following guidelines approved by the American Veterinary Medical
374 Association.

375 Female, Hartley strain guinea pigs weighing 250–350 g were obtained from Charles River
376 Laboratories and housed by Emory University Department of Animal Resources. Before intranasal
377 inoculation and nasal washing, the guinea pigs were anaesthetized with 30 mg kg⁻¹ ketamine and
378 4 mg kg⁻¹ xylazine by intramuscular injection. The G_{PID₅₀} of the NL09 virus was previously
379 determined to be 1x10¹ PFU³². To evaluate reassortment kinetics in guinea pigs, groups of six
380 animals were infected with 1x10³ PFU (1x10² ID₅₀) or 1x10⁶ PFU (1x10⁵ ID₅₀) of the NL09 WT/VAR
381 virus mixtures. Virus inoculum was given intranasally in a 300 µl volume of PBS. Nasal washes
382 were performed on days 1–6 post-inoculation and titrated by plaque assay. Viral genotyping was
383 performed on samples collected on days 1, 2 and 3 or 4 for each guinea pig. Day 3 was used for
384 animals receiving the higher dose since virus is cleared rapidly in this system and shedding has
385 ceased by day 4.

386 Female ferrets, 20-weeks-old, from Triple F Farms (Gillett, PA) were used. All ferrets were
387 seronegative by anti-nucleoprotein (anti-NP) influenza virus enzyme-linked immunosorbent
388 assay, Swine Influenza Virus Ab Test, (IDEXX, Westbrook, ME) prior to infection. Five days prior
389 to experimentation, ferrets were sedated, and a subcutaneous transponder (Bio Medic Data
390 Systems, Seaford, Delaware) was implanted to identify each animal and provide temperature
391 readings. Anesthetics were applied via intramuscular injection with ketamine (20 mg kg⁻¹) and
392 xylazine (1 mg kg⁻¹). Infections were performed via intranasal inoculation of 1 mL of virus diluted
393 in PBS. Ferret nasal washes were carried out as follows. Ferrets were anesthetized and 1 ml of
394 PBS administered to the nose was used to induce sneezing. Expelled fluid was collected into Petri
395 dishes and samples were collected in an additional volume of 1 mL PBS. Infected ferrets were
396 monitored daily for clinical signs, temperature and weight loss. Ferrets were euthanized by
397 intravenous injection of 1 ml of Beuthanasia-D diluted 1:1 with DI water (Merck, Madison, NJ).
398 For determination of ferret ID₅₀, six groups of four ferrets each were inoculated with increasing
399 doses of the NL09 WT/VAR virus mixture (1x10^{0.1} PFU, 1x10⁰ PFU, 1x10¹ PFU, 1x10² PFU, 1x10³
400 PFU and 1x10⁴ PFU). Nasal washes were collected daily for up to 6 days and titrated for viral

401 shedding by plaque assay. The ferret ID₅₀ was determined based on results obtained at day 2 and
402 found to be equivalent to 3.2×10^2 PFU.

403 For analysis of reassortment frequency and detection of viral antigen in tissues, ferrets were
404 inoculated with 3.2×10^4 PFU (1×10^2 ID₅₀) or 3.2×10^7 PFU (1×10^5 ID₅₀). After infections, nasal
405 washes were collected daily for up to 6 days and titrated by plaque assay. Viral genotyping was
406 performed on samples collected on days 1, 3 and 5 for each ferret. Necropsies were performed
407 on days 1–4 for collection of nasal turbinate and lung tissues. A single lung lobe (the left caudal
408 lobe) was sampled from each ferret. Tissue sections collected for virology were disrupted in 1 mL
409 of sterile PBS using the TissueLyser LT (Qiagen, Germantown, MD) at 30 Hz for 5 min twice, in
410 microcentrifuge tubes with 3 mm Tungsten Carbide Beads (Qiagen, St. Louis, MO). Supernatants
411 were clarified by centrifugation and frozen at -80°C until viral titration. For histology, tissues were
412 submerged in 10% buffered formalin (Sigma Aldrich, St. Louis, MO) and stored at room
413 temperature until evaluation.

414 The pig study was conducted at the Large Animal Research Center (a biosafety level 2+ facility)
415 at Kansas State University in accordance with the Guide for the Care and Use of Agricultural
416 Animals in Research and Teaching of the U.S. Department of Agriculture. To determine virus
417 reassortment and viral antigen in tissues, eighteen 4-week-old influenza H1 and H3 subtype virus-
418 and porcine reproductive and respiratory syndrome virus-seronegative gender-mixed crossbred
419 pigs were randomly allocated into groups. Each pig was inoculated with 2×10^6 PFU of NL09
420 WT/VAR mixture through both intranasal and intratracheal routes (10^6 PFU was administered in
421 a 1 ml volume by each of these two routes) under anaesthesia as described previously⁵⁴. Clinical
422 signs for all experimental pigs were monitored daily throughout the experiment. Nasal swabs
423 were collected at 1-, 3-, 5- and 7-days post infection from each pig. Three infected pigs were
424 euthanized at 3-, 5-, and 7-days post infection. During necropsy, nasal turbinate, trachea and lung
425 tissues from 7 lobes collected from each pig were frozen at -80°C for virus isolation and fixed in
426 10% buffered formalin for IHC examination.

427

428 **Quantification of reassortment.** Reassortment frequencies were evaluated by genotyping 21
429 clonal viral isolates per sample as described previously⁵⁰. This analysis was applied to guinea pig

430 nasal washes, ferret nasal washes, swine nasal swabs, ferret tissue homogenates and swine tissue
431 homogenates. Time points to be examined were chosen based on positivity in all animals in a
432 treatment group. Thus, nasal wash samples from days 1, 2, 3 or 4 were evaluated from guinea
433 pigs while samples from days 1, 3 and 5 were evaluated for swine and ferrets. Ferret tissues
434 collected on days 1, 2, 3 and 4 and swine tissues collected on days 3 and 5 were analyzed.
435 Briefly, plaque assays were performed on MDCK cells in 10 cm dishes to isolate virus clones.
436 Serological pipettes (1 ml) were used to collect agar plugs into 160 μ l PBS. Using a ZR-96 viral RNA
437 kit (Zymo), RNA was extracted from the agar plugs and eluted in 40 μ l nuclease-free water
438 (Invitrogen). Reverse transcription was performed using Maxima reverse transcriptase (RT;
439 ThermoFisher) according to the manufacturer's protocol. The resulting cDNA was diluted 1:4 in
440 nuclease-free water and each cDNA was combined with segment-specific primers^{24,31} designed
441 to amplify a region of approximately 100 base pairs. The amplicon for each segment contains the
442 site of the single nucleotide change in the VAR virus. Quantitative PCR was performed with
443 Precision Melt Supermix (Bio-Rad) using a CFX384 Touch Real-Time PCR Detection System (Bio-
444 Rad). Template amplification was followed by high-resolution melt analysis to differentiate the
445 WT and VAR amplicons⁵⁵. Precision Melt Analysis software (Bio-Rad) was used to determine the
446 parental origin of each gene segment based on the melting properties of the cDNA amplicons
447 relative to WT and VAR controls. Each plaque was assigned a genotype based on the combination
448 of WT and VAR genome segments, with two variants on each of eight segments allowing for 256
449 potential genotypes.

450

451 **Immunohistochemistry and imaging.** Tissue samples from nasal turbinates of ferrets, the right
452 caudal lung lobe of ferrets and all seven lung lobes of swine were fixed in 10% neutral buffered
453 formalin for at least 24 h before being embedded in paraffin. Nasal turbinates were decalcified
454 prior to being embedded in paraffin. Sections from all the tissues were cut and slides were
455 prepared. The tissues were deparaffinized by warming the slides at 60°C on a slide warmer for
456 45 min followed by immersion in xylenes (Sigma) for 25 min. The slides were then immersed in
457 100% ethanol for 10 min, 95% ethanol for 10 min and 70% ethanol for 5 min. The slides were
458 then washed by placing in deionized water for 1 h. Antigen retrieval was performed by steaming

459 the slides in 10 mM citric acid, pH 6.0 for 45 min, followed by washing in tap water and 1X PBS
460 (Corning) for 5 min. The WT and VAR viruses were detected in the tissues using a mouse anti HA
461 Alexa Fluor 488 (Invitrogen catalogue number A-21287; clone 16B12) and mouse anti His Alexa
462 Fluor 555 (Invitrogen catalogue number MA1-135-A555; clone 4E3D10H2/E3) while epithelial cell
463 borders were stained using rabbit anti Na^+/K^+ ATPase Alexa Fluor 647 (Abcam catalogue number
464 198367; clone EP1845Y) at 4°C overnight. Slides were washed three times in 1X PBS (Corning)
465 and once in deionized water to remove excess antibody. The slides were mounted onto glass
466 coverslips using ProLong Diamond Anti Fade mounting media (ThermoFisher). The images were
467 acquired using an Olympus FV1000 Confocal Microscope at 60x magnification under an oil
468 immersion objective. The specificity of the antibodies was confirmed by infecting MDCK cells with
469 either the NL09 WT, NL09 VAR or both viruses for 24 h. The cells were fixed using 4%
470 paraformaldehyde (Alfa Aesar) and stained for HA and His tags using the antibodies as described
471 above (Supplementary Fig. 9).

472 For morphological analysis via IHC, the slides were pre-treated in pH 9.0 buffer at 110°C for 15
473 minutes. Blocking was performed using hydrogen peroxide for 20 minutes followed by
474 PowerBlock (BioGenex) for 5 minutes. Slides were washed with PBS thrice and NP antigen was
475 detected using a goat anti-influenza NP polyclonal antibody (abcam catalogue number ab155877)
476 for 1 h. Slides were washed thrice with PBS to remove excess antibody and incubated with a
477 rabbit anti-goat biotinylated IgG (Vector laboratories catalogue number BA-5000) for 10 minutes.
478 After washing, 4Plus Alkaline Phosphatase Label (BioCare Medical) was added for 10 minutes.
479 The antigen signal was detected by incubating the slides in Chromogen IP Warp Red stain
480 (BioCare Medical) for 10 minutes. Haematoxylin counterstaining was performed post antigen
481 staining.

482

483 **Software**

484 Figures were generated using Python 3⁵⁶ and the packages matplotlib⁵⁷, NumPy⁵⁸, pandas⁵⁹ and
485 seaborn⁶⁰. Simulations were conducted in Python 3.

486

487 **Analysis of genotype frequencies, richness and diversity**

488 Here a viral genotype is defined as a unique combination of the eight IAV segments, where each
489 segment is derived from either the variant or wild type parental virus; therefore, there are 2^8
490 possible unique genotypes, with two parental genotypes and 254 reassortant genotypes. For any
491 given sample, the frequency of each unique genotype can be calculated by dividing the number
492 of appearances each unique genotype has in the sample by the total number of clonal isolates
493 obtained for that sample.

494 Understanding the distribution of unique genotypes involves using both unweighted and
495 weighted genotype frequency statistics. Genotype richness (S) does not incorporate genotype
496 frequency and is given by the number of unique genotypes in a sample. Given our sample size of
497 21 plaque isolates, genotype richness, or the number of distinct genotypes detected in a sample,
498 can range from a minimum of 1 (a single genotype is detected 21 times) to a maximum of 21 (21
499 unique genotypes are detected).

500 Diversity was measured using the Shannon-Weiner index (H), which considers both richness and
501 evenness in the frequency with which genotypes are detected. In our dataset, diversity can range
502 from 0 to 3.04. Shannon-Wiener diversity was calculated as:

$$503 \quad H = - \sum_{i=1}^S (p_i * \ln p_i)$$

504 where S is genotype richness and p_i is the frequency of unique genotype i in the sample (6).

505 To address whether evaluating 21 plaques per sample for this analysis was sufficient to yield
506 robust results on genotype diversity, we used a computational simulation to test the sensitivity
507 of the measured diversity values to the number of plaques sampled. In these simulations, we
508 calculated the diversity present in samples generated by randomly picking n (out of the possible
509 21) plaques without replacement. At each sampling effort n , we simulated 1000 samples, with
510 plaque replacement between samples. The results typically show that diversity values increase
511 as n increases, with values asymptoting as n approaches 21, suggesting that further increases in
512 n would not greatly change results and validating the use of 21 plaques (Supplementary Fig. 10).
513 To evaluate the extent to which the spatial dynamics of viral reassortment and propagation shape
514 the overall richness and diversity in a host, we sought to compare the observed richness and
515 diversity at each anatomical site to that which would be expected if virus moves freely among

516 anatomical locations. Thus, to simulate free mixing within the host, we randomly shuffled
517 observed viral genotypes among all sites in a given animal. The average richness and Shannon-
518 Wiener index of the simulated viral populations at each site were then calculated. The 5th and
519 95th percentiles for the simulated distribution of each animal were calculated and compared to
520 the observed richness and diversity for each of the anatomical sites. If a site's observed richness
521 and diversity fell below the 5th percentile or above the 95th percentile, then a barrier to the influx
522 or efflux of reassortant genotypes from or to the other sites is suggested.

523

524 **Analysis of beta diversity**

525 The dissimilarity between populations can be measured by beta diversity. For this study, we
526 evaluated beta diversity from a richness perspective, focusing on dissimilarity in the unique
527 genotypes detected and excluding consideration of their frequency. This approach was used to
528 de-emphasize the effects of WT and VAR parental genotypes, which were likely seeded into all
529 anatomical locations at the time of inoculation. We calculate the beta diversity by treating the
530 viral genotypes in two lobes as two distinct populations:

$$531 \quad \beta = \frac{S_{1+2}}{\frac{1}{2}(S_1 + S_2)}$$

532 where S_{1+2} is the richness of a hypothetical population composed of pooling the viral genotypes
533 of the two lobes while $\frac{1}{2}(S_1 + S_2)$ represents the mean richness of the lobes
534 (7). The beta diversity of a single comparison can be normalized so that it ranges from zero to
535 one:

$$536 \quad BD' = \frac{BD - 1}{BD_{max} - 1} \beta_n$$

537 where BD_{max} is the beta diversity calculated by assuming that there are no viral genotypes
538 shared by both lobes (7). A $BD' \beta_n$ closer to one indicates that the lobes' viral populations are
539 more dissimilar while a $BD' \beta_n$ closer to zero suggests that the lobes have similar unique viral
540 genotypes and overall viral richness. A $BD' \beta_n$ of zero occurs when all unique genotypes present
541 in one lobe are also present in the other.

542 To address whether evaluating 21 plaques per sample for this analysis was sufficient to yield
543 robust results on beta diversity, we again used computational simulations. These simulations
544 were designed to test the sensitivity of beta diversity values to the number of plaques sampled.
545 In these simulations, we again generated plaque data subsets by randomly picking n (out of the
546 possible 21) plaques without replacement. At each sampling effort n , we simulated 1000 samples,
547 with plaque replacement between samples. Beta diversity values were then calculated based on
548 these data subsets, at a given n . The results typically show that β_n values tend to stabilize as n
549 approaches 21, suggesting that further increases in n would not greatly change results and
550 validating the use of 21 plaques (Supplementary Fig. 10). In a subset of cases that involve the
551 nasal sample of Pig 5, however, the relationship between β_n and n is less stable. In sharp contrast
552 to most other samples from Pig 5, the nasal site showed 20 WT parental isolates and one VAR
553 parental isolate. The lung tissues had no WT parental genotypes detected. As a result, each
554 successive plaque draw from the nasal sample increases the probability of detecting the VAR
555 virus and therefore detecting a commonality between the nasal tract and any of the lung lobes.
556 Thus, in situations where two tissue sites have a single, relatively rare genotype in common, the
557 number of plaques sampled has a strong impact on β_n outcomes.
558 To simulate free mixing between two lobes, we randomly shuffled the genotypes between each
559 of the 28 pairwise combinations among pig tissues and the single ferret lung-NT combination and
560 computed the $BD'\beta_n$ for each comparison. Free mixing for all combinations was simulated 1000
561 times. We reasoned that if compartmentalization was present in the observed dataset, then the
562 dissimilarity values would fall at the high end of the simulated distribution (>95th percentile).
563

564 **Statistical measures**

565 Percentiles were calculated using the percentileofscore method from the SciPy package⁵⁹. Paired
566 t-tests and ANOVA tests were performed using the ttest_rel method and the f_oneway method
567 respectively from the SciPy Package⁵⁹.

568

569 **Data availability**

570 Raw data are included as Source Data and in Supplementary Table 1.

571

572 **Code availability**

573 Code used for data analysis and simulations is available at:

574 <https://github.com/maxbagga/Influenza-A-virus-reassortment-in-mammals-gives-rise-to-spatially-distinct-sub-populations>

576

577 **Acknowledgements**

578 We thank Shamika Danzy for technical assistance. We would like to thank the Emory Division of
579 Animal Resources for their assistance with the guinea pig experiments. We thank Rusty
580 Ransburgh, Baoliang Zheng, Dongchang He, Abaineh Endalew, Daniel Madden, Yuekun Lang for
581 their assistance with the pig experiments. This project was supported by the Emory University
582 Integrated Cellular Imaging Microscopy Core. The research was funded by NIH R01 AI127799 and
583 the NIH/NIAID Centers of Excellence in Influenza Research and Response (CEIRR), contract
584 numbers 75N93021C00017 (ACL, KK), 75N93021C00014 (DRP) and 75N93021C00016 (JAR, WM),
585 and the AMP Core of the Center of Emerging and Zoonotic Infectious Diseases (CEZID) from
586 NIGMS under award number P20GM130448 (JAR).

587

588 **References**

589

- 590 1 Webster, R. G., Hinshaw, V. S., Bean, W. J., Jr., Turner, B. & Shortridge, K. F. Influenza
591 viruses from avian and porcine sources and their possible role in the origin of human
592 pandemic strains. *Dev Biol Stand* **39**, 461-468 (1977).
- 593 2 Wright, P. F., Neumann, G. & Kawaoka, Y. in *Fields Virology* Vol. 1 (ed D. M. & Howley
594 Knipe, P. M.) 1691-1740 (Lippincott-Raven, 2006).
- 595 3 Webster, R. G., Bean, W. J., Gorman, O. T., Chambers, T. M. & Kawaoka, Y. Evolution and
596 ecology of influenza A viruses. *Microbiol Rev* **56**, 152-179 (1992).
- 597 4 Webster, R. G., Shortridge, K. F. & Kawaoka, Y. Influenza: interspecies transmission and
598 emergence of new pandemics. *FEMS Immunol Med Microbiol* **18**, 275-279, doi:S0928-
599 8244(97)00058-8 [pii] (1997).
- 600 5 Taubenberger, J. K. & Morens, D. M. 1918 Influenza: the mother of all pandemics. *Emerg
601 Infect Dis* **12**, 15-22 (2006).
- 602 6 Viboud, C., Miller, M., Olson, D., Osterholm, M. & Simonsen, L. Preliminary Estimates of
603 Mortality and Years of Life Lost Associated with the 2009 A/H1N1 Pandemic in the US and

604 605 Comparison with Past Influenza Seasons. *PLoS Curr*, RRN1153, doi:k/-/-
/35hpbywfdwl4n/8 [pii] (2010).

606 7 Ma, E. J., Hill, N. J., Zabilansky, J., Yuan, K. & Runstadler, J. A. Reticulate evolution is
607 favored in influenza niche switching. *Proc Natl Acad Sci U S A* **113**, 5335-5339,
608 doi:10.1073/pnas.1522921113 (2016).

609 8 Kilbourne, E. D. Influenza pandemics of the 20th century. *Emerg Infect Dis* **12**, 9-14 (2006).

610 9 Smith, G. J. *et al.* Origins and evolutionary genomics of the 2009 swine-origin H1N1
611 influenza A epidemic. *Nature* **459**, 1122-1125, doi:10.1038/nature08182 (2009).

612 10 Nelson, M. I. & Vincent, A. L. Reverse zoonosis of influenza to swine: new perspectives on
613 the human-animal interface. *Trends Microbiol* **23**, 142-153,
614 doi:10.1016/j.tim.2014.12.002 (2015).

615 11 Woods, G. T., Schnurrenberger, P. R., Martin, R. J. & Tompkins, W. A. Swine influenza virus
616 in swine and man in Illinois. *J Occup Med* **23**, 263-267 (1981).

617 12 Ma, W. *et al.* Identification of H2N3 influenza A viruses from swine in the United States.
618 *Proc Natl Acad Sci U S A* **104**, 20949-20954, doi:10.1073/pnas.0710286104 (2007).

619 13 Ma, W., Kahn, R. E. & Richt, J. A. The pig as a mixing vessel for influenza viruses: Human
620 and veterinary implications. *J Mol Genet Med* **3**, 158-166 (2008).

621 14 Kahn, R. E., Ma, W. & Richt, J. A. Swine and influenza: a challenge to one health research.
622 *Curr Top Microbiol Immunol* **385**, 205-218, doi:10.1007/82_2014_392 (2014).

623 15 Rajao, D. S. *et al.* Reassortment between Swine H3N2 and 2009 Pandemic H1N1 in the
624 United States Resulted in Influenza A Viruses with Diverse Genetic Constellations with
625 Variable Virulence in Pigs. *J Virol* **91**, doi:10.1128/JVI.01763-16 (2017).

626 16 Nelson, M. I. *et al.* Genomic reassortment of influenza A virus in North American swine,
627 1998-2011. *J Gen Virol* **93**, 2584-2589, doi:10.1099/vir.0.045930-0 (2012).

628 17 Lam, T. T. *et al.* Reassortment events among swine influenza A viruses in China:
629 implications for the origin of the 2009 influenza pandemic. *J Virol* **85**, 10279-10285,
630 doi:10.1128/JVI.05262-11 (2011).

631 18 Zhou, N. N. *et al.* Genetic reassortment of avian, swine, and human influenza A viruses in
632 American pigs. *J Virol* **73**, 8851-8856, doi:10.1128/JVI.73.10.8851-8856.1999 (1999).

633 19 Ma, J. *et al.* Virus survival and fitness when multiple genotypes and subtypes of influenza
634 A viruses exist and circulate in swine. *Virology* **532**, 30-38, doi:10.1016/j.virol.2019.03.016
635 (2019).

636 20 Ganti, K. *et al.* Avian Influenza A Viruses Reassort and Diversify Differently in Mallards and
637 Mammals. *Viruses* **13**, doi:10.3390/v13030509 (2021).

638 21 Tao, H., Li, L., White, M. C., Steel, J. & Lowen, A. C. Influenza A Virus Coinfection through
639 Transmission Can Support High Levels of Reassortment. *J Virol* **89**, 8453-8461,
640 doi:10.1128/JVI.01162-15 (2015).

641 22 Tao, H., Steel, J. & Lowen, A. C. Intrahost dynamics of influenza virus reassortment. *J Virol*
642 **88**, 7485-7492, doi:10.1128/JVI.00715-14 (2014).

643 23 Richard, M., Herfst, S., Tao, H., Jacobs, N. T. & Lowen, A. C. Influenza A Virus Reassortment
644 Is Limited by Anatomical Compartmentalization following Coinfection via Distinct Routes.
645 *J Virol* **92**, doi:10.1128/JVI.02063-17 (2018).

646 24 Phipps, K. L. *et al.* Collective interactions augment influenza A virus replication in a host-
647 dependent manner. *Nat Microbiol* **5**, 1158-1169, doi:10.1038/s41564-020-0749-2 (2020).

648 25 Amato, K. A. *et al.* Influenza A virus undergoes compartmentalized replication in vivo
649 dominated by stochastic bottlenecks. *Nat Commun* **13**, 3416, doi:10.1038/s41467-022-
650 31147-0 (2022).

651 26 Richard, M. *et al.* Influenza A viruses are transmitted via the air from the nasal respiratory
652 epithelium of ferrets. *Nat Commun* **11**, 766, doi:10.1038/s41467-020-14626-0 (2020).

653 27 Xie, C. *et al.* A(H1N1)pdm09 Influenza Viruses Replicating in Ferret Upper or Lower
654 Respiratory Tract Differed in Onward Transmission Potential by Air. *J Infect Dis* **225**, 65-
655 74, doi:10.1093/infdis/jiab286 (2022).

656 28 Belser, J. A., Katz, J. M. & Tumpey, T. M. The ferret as a model organism to study influenza
657 A virus infection. *Dis Model Mech* **4**, 575-579, doi:10.1242/dmm.007823 (2011).

658 29 Danzy, S., Lowen, A. C. & Steel, J. A quantitative approach to assess influenza A virus
659 fitness and transmission in guinea pigs. *J Virol*, doi:10.1128/JVI.02320-20 (2021).

660 30 Lowen, A. C., Bouvier, N. M. & Steel, J. Transmission in the guinea pig model. *Curr Top*
661 *Microbiol Immunol* **385**, 157-183, doi:10.1007/82_2014_390 (2014).

662 31 Phipps, K. L. *et al.* Seasonal H3N2 and 2009 Pandemic H1N1 Influenza A Viruses Reassort
663 Efficiently but Produce Attenuated Progeny. *J Virol* **91**, doi:10.1128/JVI.00830-17 (2017).

664 32 Campbell, P. J. *et al.* The M segment of the 2009 pandemic influenza virus confers
665 increased neuraminidase activity, filamentous morphology, and efficient contact
666 transmissibility to A/Puerto Rico/8/1934-based reassortant viruses. *J Virol* **88**, 3802-3814,
667 doi:10.1128/JVI.03607-13 (2014).

668 33 Jasinska, W. *et al.* Chromosomal barcoding of *E. coli* populations reveals lineage diversity
669 dynamics at high resolution. *Nat Ecol Evol* **4**, 437-452, doi:10.1038/s41559-020-1103-z
670 (2020).

671 34 Matrosovich, M. N., Matrosovich, T. Y., Gray, T., Roberts, N. A. & Klenk, H. D. Human and
672 avian influenza viruses target different cell types in cultures of human airway epithelium.
673 *Proc Natl Acad Sci U S A* **101**, 4620-4624, doi:10.1073/pnas.0308001101 (2004).

674 35 van Riel, D. *et al.* Novel avian-origin influenza A (H7N9) virus attaches to epithelium in
675 both upper and lower respiratory tract of humans. *Am J Pathol* **183**, 1137-1143,
676 doi:10.1016/j.ajpath.2013.06.011 (2013).

677 36 Mifsud, E. J., Kuba, M. & Barr, I. G. Innate Immune Responses to Influenza Virus Infections
678 in the Upper Respiratory Tract. *Viruses* **13**, doi:10.3390/v13102090 (2021).

679 37 Brooke, C. B., Ince, W. L., Wei, J., Bennink, J. R. & Yewdell, J. W. Influenza A virus
680 nucleoprotein selectively decreases neuraminidase gene-segment packaging while
681 enhancing viral fitness and transmissibility. *Proc Natl Acad Sci U S A* **111**, 16854-16859,
682 doi:10.1073/pnas.1415396111 (2014).

683 38 Brooke, C. B. *et al.* Most influenza A virions fail to express at least one essential viral
684 protein. *J Virol* **87**, 3155-3162, doi:10.1128/JVI.02284-12 (2013).

685 39 Jacobs, N. T. *et al.* Incomplete influenza A virus genomes occur frequently but are readily
686 complemented during localized viral spread. *Nat Commun* **10**, 3526, doi:10.1038/s41467-
687 019-11428-x (2019).

688 40 Ganti, K., Han, J., Manicassamy, B. & Lowen, A. C. Rab11a mediates cell-cell spread and
689 reassortment of influenza A virus genomes via tunneling nanotubes. *PLoS Pathog* **17**,
690 e1009321, doi:10.1371/journal.ppat.1009321 (2021).

691 41 Sobel Leonard, A. *et al.* The effective rate of influenza reassortment is limited during
692 human infection. *PLoS Pathog* **13**, e1006203, doi:10.1371/journal.ppat.1006203 (2017).

693 42 Gallagher, M. E., Brooke, C. B., Ke, R. & Koelle, K. Causes and Consequences of Spatial
694 Within-Host Viral Spread. *Viruses* **10**, doi:10.3390/v10110627 (2018).

695 43 Lakdawala, S. S. *et al.* The soft palate is an important site of adaptation for transmissible
696 influenza viruses. *Nature* **526**, 122-125, doi:10.1038/nature15379 (2015).

697 44 Zaraket, H. *et al.* Mammalian adaptation of influenza A(H7N9) virus is limited by a narrow
698 genetic bottleneck. *Nat Commun* **6**, 6553, doi:10.1038/ncomms7553 (2015).

699 45 Zwart, M. P. & Elena, S. F. Matters of Size: Genetic Bottlenecks in Virus Infection and Their
700 Potential Impact on Evolution. *Annu Rev Virol* **2**, 161-179, doi:10.1146/annurev-virology-
701 100114-055135 (2015).

702 46 Vijaykrishna, D. *et al.* Reassortment of pandemic H1N1/2009 influenza A virus in swine.
703 *Science* **328**, 1529, doi:10.1126/science.1189132 (2010).

704 47 Mine, J., Uchida, Y., Takemae, N. & Saito, T. Genetic Characterization of Influenza A
705 Viruses in Japanese Swine in 2015 to 2019. *J Virol* **94**, doi:10.1128/JVI.02169-19 (2020).

706 48 Gao, S. *et al.* The genomic evolution of H1 influenza A viruses from swine detected in the
707 United States between 2009 and 2016. *J Gen Virol* **98**, 2001-2010,
708 doi:10.1099/jgv.0.000885 (2017).

709 49 White, M. C. & Lowen, A. C. Implications of segment mismatch for influenza A virus
710 evolution. *J Gen Virol* **99**, 3-16, doi:10.1099/jgv.0.000989 (2018).

711 50 Marshall, N., Priyamvada, L., Ende, Z., Steel, J. & Lowen, A. C. Influenza virus reassortment
712 occurs with high frequency in the absence of segment mismatch. *PLoS Pathog* **9**,
713 e1003421, doi:10.1371/journal.ppat.1003421 (2013).

714 51 Fodor, E. *et al.* Rescue of influenza A virus from recombinant DNA. *J Virol* **73**, 9679-9682,
715 doi:10.1128/JVI.73.11.9679-9682.1999 (1999).

716 52 Hoffmann, E., Neumann, G., Hobom, G., Webster, R. G. & Kawaoka, Y. "Ambisense"
717 approach for the generation of influenza A virus: vRNA and mRNA synthesis from one
718 template. *Virology* **267**, 310-317, doi:10.1006/viro.1999.0140 (2000).

719 53 Chutinimitkul, S. *et al.* Virulence-associated substitution D222G in the hemagglutinin of
720 2009 pandemic influenza A(H1N1) virus affects receptor binding. *J Virol* **84**, 11802-11813,
721 doi:10.1128/JVI.01136-10 (2010).

722 54 Richt, J. A. *et al.* Pathogenic and antigenic properties of phylogenetically distinct
723 reassortant H3N2 swine influenza viruses cocirculating in the United States. *J Clin
724 Microbiol* **41**, 3198-3205, doi:10.1128/JCM.41.7.3198-3205.2003 (2003).

725 55 Wittwer, C. T., Reed, G. H., Gundry, C. N., Vandersteen, J. G. & Pryor, R. J. High-resolution
726 genotyping by amplicon melting analysis using LCGreen. *Clin Chem* **49**, 853-860,
727 doi:10.1373/49.6.853 (2003).

728 56 Van Rossum, G. & Drake, F. L. *Python 3 Reference Manual*. (CreateSpace, 2009).

729 57 Hunter, J. D. Matplotlib: A 2D Graphics Environment. *Computing in Science & Engineering*
730 **9**, 90-95, doi:doi: 10.1109/MCSE.2007.55 (2007).

731 58 Oliphant, T. E. *A guide to NumPy* Vol. 1 (Trelgol Publishing, 2006).

732 59 McKinney, W. Data structures for statistical computing in python. *Proceedings of the 9th
733 Python in Science Conference* **445**, 51-56 (2010).

734 60 Waskom, M. L. seaborn: statistical data visualization. *Journal of Open Source Software* **6**,
735 3021, doi:doi:10.21105/joss.03021 (2021).

736

737

738 **Figure Legends**

739 **Figure 1: Viral genotypic diversity generated through reassortment in the mammalian nasal**
740 **tract.** Results from guinea pigs are shown in panels A–D, ferrets in panels E–H and swine in panels
741 I–L. Stacked plots (A, E, I) show frequencies of unique genotypes detected in one representative
742 animal over time. Blue and orange represent the WT and VAR parental genotypes, respectively.
743 Frequency of both parental genotypes combined (B, F, J), richness (C, G, K) and Shannon-Weiner
744 diversity (D, H, L) are each plotted as a function of time. Guinea pigs and ferrets inoculated at
745 high dose (1×10^5 ID₅₀) and low dose (1×10^2 ID₅₀) are indicated with dashed and solid lines,
746 respectively. The distribution of parental genotype frequencies (M), richness (N) and diversity (O)
747 across all time points in each species is shown with violin plots. Differences in richness and
748 diversity between swine and guinea pigs and between swine and ferrets were significant ($p < 0.01$,
749 ANOVA). Parental genotype frequencies differed significantly between swine and guinea pigs
750 ($p = 0.003$, ANOVA), and were not significant between swine and ferrets ($p > 0.05$, ANOVA).

751

752 **Figure 2: Viral diversity generated through reassortment is greater in the ferret nasal turbinates**
753 **than in the lungs.** Pie charts show frequencies of unique genotypes detected in the nasal
754 turbinates (NT) and lung of ferrets inoculated with 1×10^2 FID₅₀ (A) or 1×10^5 FID₅₀ (B). Ferrets
755 shown were analyzed at the following times post-infection: Day 1 (F11, 12, 19, 20), Day 2 (F13,
756 14, 21, 22), Day 3 (F15, 16, 23) and Day 4 (F17, 18, 24). Blue and orange sections of the pie charts
757 represent VAR and WT parental genotypes, respectively. Richness (C) and diversity (D) are
758 plotted, with observed results (colored points) overlaid on the distribution of simulated data
759 (grey violins). Horizontal lines denote the 95th and 5th percentiles. The distribution of richness (E)
760 and diversity (F) in NT and lungs of all individuals is shown with violin plots. Differences between
761 NT and lungs were significant by both measures ($p < 0.01$, paired t-test).

762

763 **Figure 3: Reassortant viral populations in the ferret upper and lower respiratory tracts are**
764 **distinct.** Heat map showing normalized beta diversity of viral populations in ferret lung and nasal
765 turbinates (NT) (A). The inset shows a representative comparison between the tissues of ferrets
766 F23 and F21, to indicate the position of NT and lung within the matrix. Normalized beta diversity
767 is plotted in (B) with observed results (colored points) overlaid on the distribution of simulated
768 data (gray violins). One star indicates that observed data is above the 95th percentile of the
769 distribution; two stars indicates that observed data is above the 99th percentile. (C)
770 Immunohistochemistry images of ferret F23 NT and lung sections stained for WT (green) and VAR
771 (red) viruses at day 3 post-inoculation. Gray staining marks epithelial cell borders. Yellow coloring
772 in merged images indicates the presence of both WT and VAR HA antigens in the same cell.
773 Zoomed insets of both NT and lung sections are shown with white arrows indicating co-infected
774 cells and yellow arrows indicating singly infected cells. Scale bars are 20 μ m. (D)
775 Immunohistochemistry images of ferret F24 lung sections stained for nucleoprotein (red) and
776 counterstained with hematoxylin. Scale bars are 20 μ m.

777

778 **Figure 4: Local diversity arising through reassortment is modest within the swine respiratory**
779 **tract.** Pie charts showing frequencies of unique genotypes present within each lung lobe of a
780 given pig on day 3 (A-C) and the nasal tract and each lung lobe of a given pig on day 5 (D-F) with
781 blue and orange sections representing WT and VAR parental genotypes, respectively. The tissue
782 sites are abbreviated as NA-Nasal; LA-Left Apical; RA-Right Apical; LC-Left Cardiac; RC-Right
783 Cardiac; LD-Left Diaphragmatic; RD-Right Diaphragmatic; IN-Intermediate (accessory). Simulated
784 richness (G) and diversity (H) are plotted, with observed results (colored points) overlaid on the
785 distribution of simulated data (grey violins). Horizontal lines denote the 95th and 5th percentiles.

786

787 **Figure 5: Reassortant viral populations show extensive compartmentalization within the swine**
788 **respiratory tract.** Heat map showing normalized beta diversity of viral populations in swine lung
789 and nasal tract (A). The inset shows a representative comparison between the tissues of pigs P3
790 and P6, to indicate the position of each tissue within the matrix. The tissue sites are abbreviated
791 as NA-Nasal; LA- Left Apical; RA- Right Apical; LC-Left Cardiac; RC-Right Cardiac; LD-Left

792 Diaphragmatic; RD-Right Diaphragmatic; IN-Intermediate (accessory). Normalized beta diversity
793 between the left apical and left cardiac lobes is plotted (B) with observed results (colored points)
794 overlaid on the distribution of simulated data (gray violins). One star indicates that observed data
795 is above the 95th percentile of the distribution; two stars indicates that observed data is above
796 the 99th percentile. (C) Representative immunohistochemistry images of swine (P76) left apical
797 lung section stained for WT (green) and VAR (red) viruses at day 3 post-inoculation. Gray staining
798 marks epithelial cell borders. Yellow coloring in merged images indicates the presence of both
799 WT and VAR HA antigens in the same cell. Zoomed insets of the lung are shown with white arrows
800 indicating co-infected cells and yellow arrows indicating singly infected cells. Scale bars are 20
801 μm . (D) Immunohistochemistry images of swine (P76) left apical lung sections stained for
802 nucleoprotein (red) and counterstained with hematoxylin. Scale bars are 20 μm .

803

804

805 **Supplementary Figure Legends**

806

807 **Supplementary Fig. 1. NL09 WT and NL09 VAR show comparable replication in MDCK cells.** Viral
808 replication from low MOI was monitored over time in three replicate culture dishes. Mean and
809 standard deviation are plotted.

810

811 **Supplementary Fig. 2. Viral loads in infected guinea pigs, ferrets and swine.** Viral shedding
812 determined by plaque assay from guinea pig nasal washes (A), ferret nasal washes (B), swine
813 nasal swabs (C), ferret nasal turbinates (D), ferret lung homogenates (E), and swine lung
814 homogenates (F) over time are shown. The horizontal dashed line represents the limit of
815 detection of the plaque assay (50 PFU/mL).

816

817 **Supplementary Fig. 3. Viral genotypic diversity generated through reassortment in the**
818 **mammalian nasal tract.** (Corresponds to Figure 1) Stacked plots showing frequencies of unique
819 genotypes detected in guinea pigs (A), ferrets (B) or swine (C) over time. The sections in blue and
820 orange represent the WT and VAR parental genotypes, respectively.

821

822 **Supplementary Fig. 4. Effects of inoculation dose on viral diversity generated through**
823 **reassortment in the nasal tract.** (Corresponds to Figure 1) Results from guinea pigs are shown in
824 panels A–C, ferrets in panels D–F. HD indicates high dose (1×10^5 ID₅₀) and LD indicates low dose
825 (1×10^2 ID₅₀) groups. The distribution of parental genotype frequencies (A, D), richness (B, E) and
826 diversity (C, F) across all time points in each species is shown with violin plots. P values were
827 determined by ANOVA.

828

829 **Supplementary Fig. 5. Reassortant viral populations show extensive compartmentalization**
830 **within the swine respiratory tract.** (Corresponds to Figure 5) Heat maps showing beta diversity
831 of viral populations in the lung lobes and nasal tract of individual pigs. Pig ID number is indicated
832 above each matrix. (A) Tissues were extracted on day 3 post-inoculation. (B) Tissues were
833 extracted on day 5 post-inoculation. The tissue sites are abbreviated as NA-Nasal; LA- Left Apical;
834 RA- Right Apical; LC-Left Cardiac; RC-Right Cardiac; LD-Left Diaphragmatic; RD-Right
835 Diaphragmatic; IN-Intermediate.

836

837 **Supplementary Fig. 6. Reassortant viral populations show extensive compartmentalization**
838 **within the swine respiratory tract.** (Corresponds to Figure 5) Normalized beta diversity between
839 each lung lobe and nasal tract (A) and between lung lobes (B) are plotted with observed results
840 (colored points) overlaid on the distribution of simulated data (gray violins). One star indicates
841 that observed data is above the 95th percentile of the distribution; two stars indicates that
842 observed data is above the 99th percentile.

843

844 **Supplementary Fig. 7. Coinfection is common in the swine respiratory tract.** (Corresponds to
845 Figure 5) Immunohistochemistry images of lung tissue sections stained for WT (green) and VAR
846 (red) viruses at day 3 post-inoculation. The lung lobe sampled is indicated at the left. Gray staining
847 marks epithelial cell borders. Yellow coloring in merged images indicates the presence of both
848 WT and VAR HA antigens in the same cell. Zoomed insets are shown with white arrows indicating
849 co-infected cells and yellow arrows indicating singly infected cells.

850

851 **Supplementary Fig. 8. Identification of infected cell types in swine respiratory tract.**
852 (Corresponds to Figure 5). Tissue sections were stained for viral nucleoprotein (red) and
853 counterstained with hematoxylin and eosin. Scale bars are 20 μ m.

854

855 **Supplementary Fig. 9. Validation of the antibodies used for immunohistochemistry.**
856 Immunofluorescence images of MDCK cells stained for WT (green) and VAR (red) viruses at 24 h
857 post infection. Gray staining marks epithelial cell borders. Yellow coloring in merged images
858 indicates the presence of both WT and VAR HA antigens in the same cell.

859

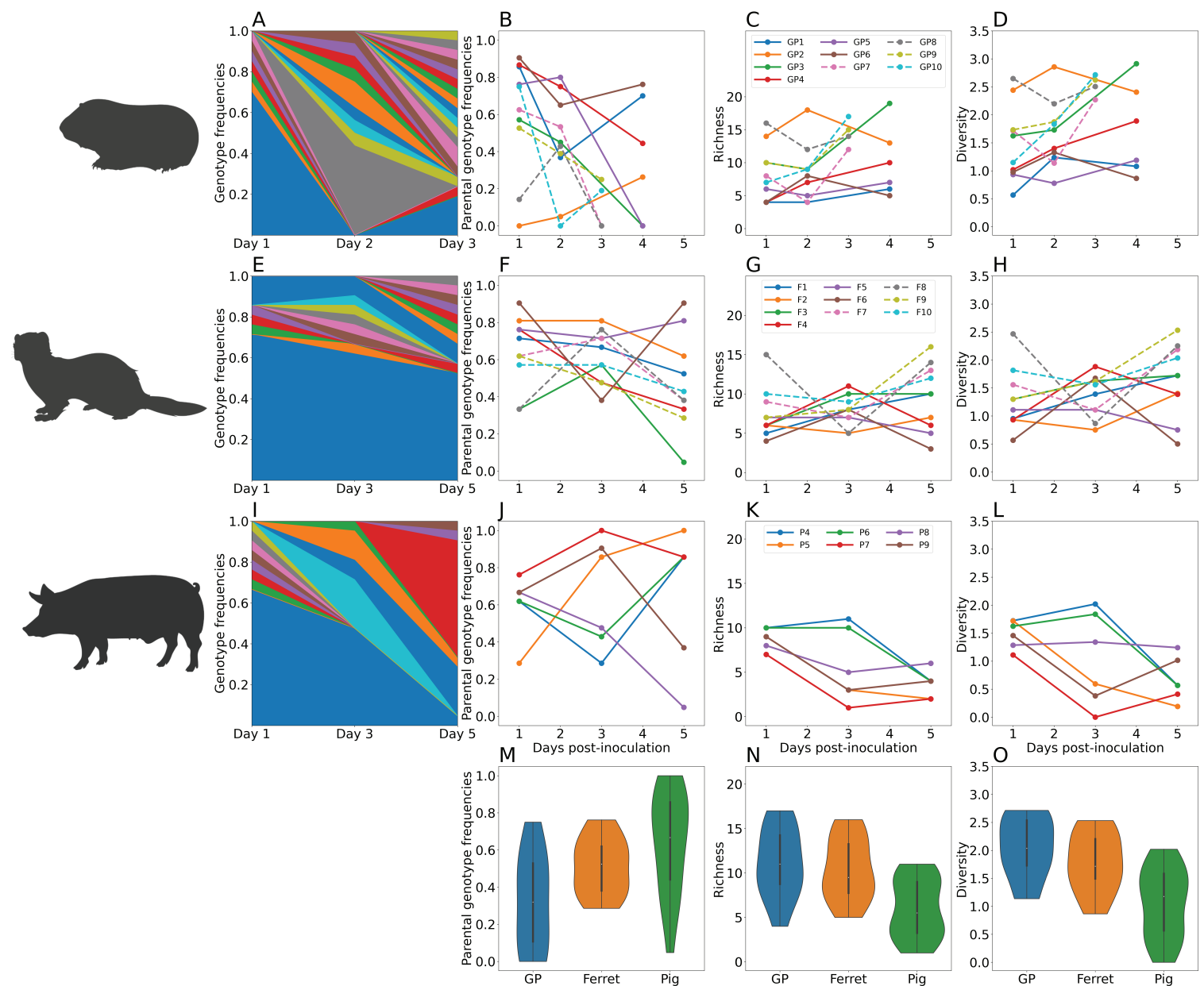
860 **Supplementary Fig. 10. Evaluation of the sensitivities of diversity and beta diversity to the**
861 **number of viral plaques analyzed.** The impact of the number of plaques analyzed on the
862 detection of diversity in guinea pigs, pigs and ferrets (A), beta diversity in ferrets (B) and beta
863 diversity in pigs (C) was assessed by sub-sampling from our experimental dataset with 1000
864 replicate simulations performed at each number of plaques. Representative samples were
865 analyzed and the sample is indicated above each facet. Points with the green triangles inside
866 indicate the mean. Boxes represent the first and third quartiles, with the middle line representing
867 the median. Whiskers show the minimum and maximum of the data with the outliers omitted
868 outside of two standard deviations (plotted by the diamonds). The red data point shows the
869 observed result reported in the main figures.

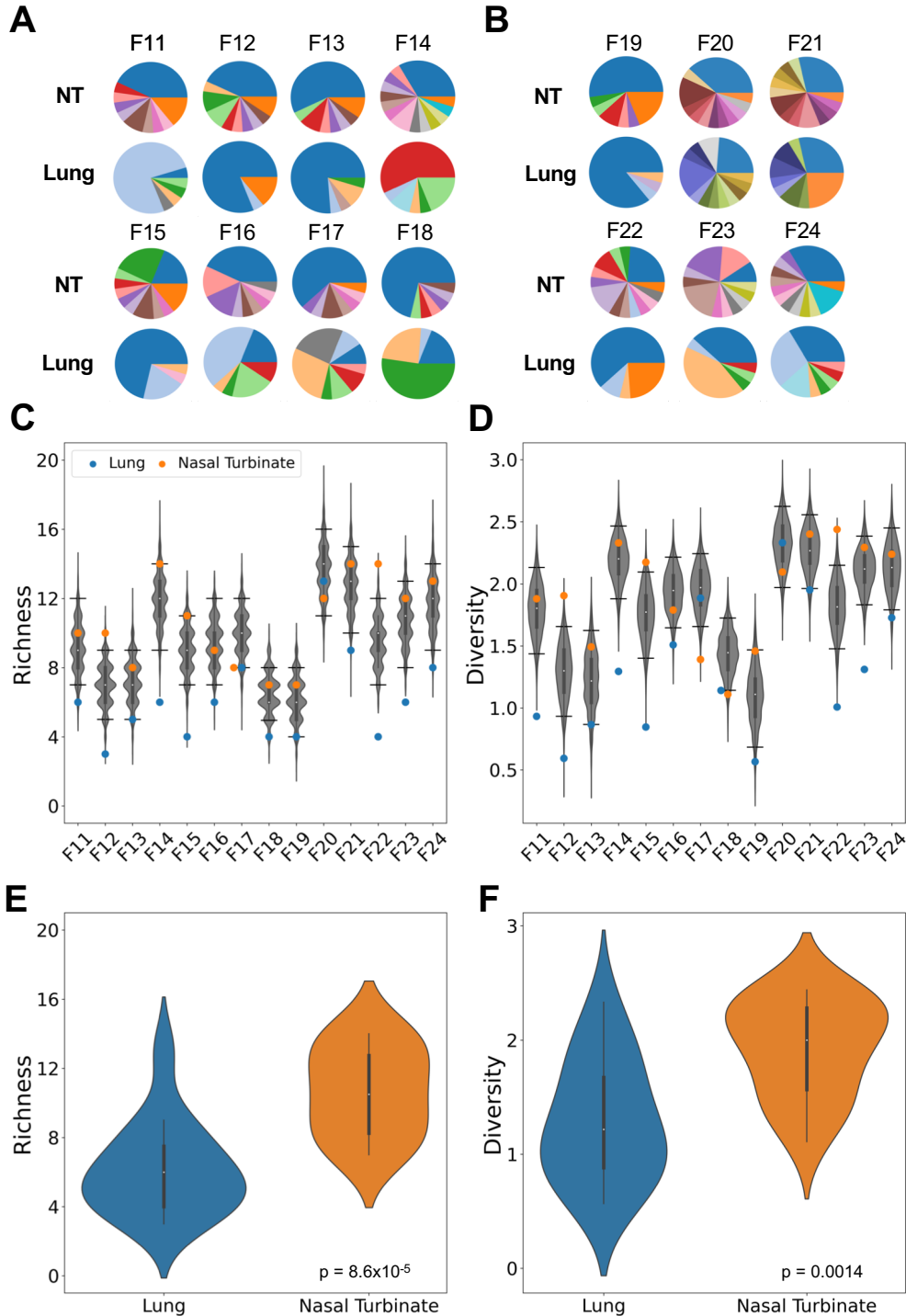
870

871 **Supplementary Table 1. Genotype tables.** Viral genotypes detected in guinea pigs, ferrets and
872 swine are included. Each table corresponds to a biological sample and each row in each table
873 corresponds to a single viral isolate. The columns show the eight viral gene segments. Blue color
874 blocks indicate WT genes while red color blocks indicate VAR genes.

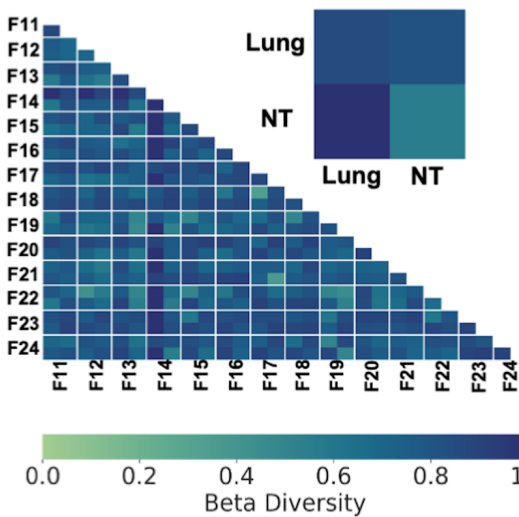
875

876 **Supplementary Table 2. Identification of viral nucleoprotein positive cells present in ferret**
877 **lung, pig lung and pig nasal turbinate.**

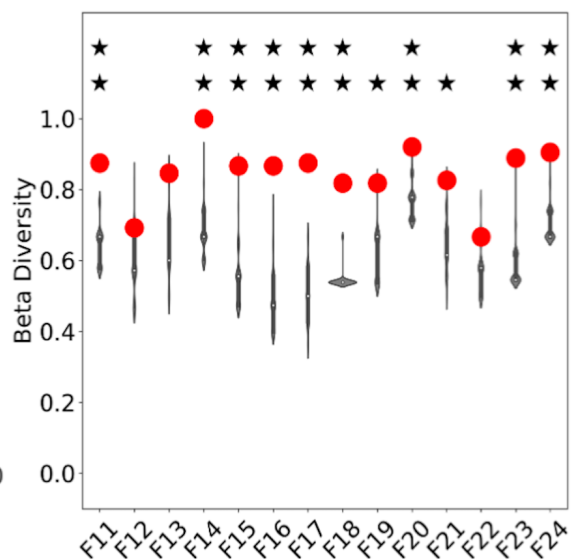




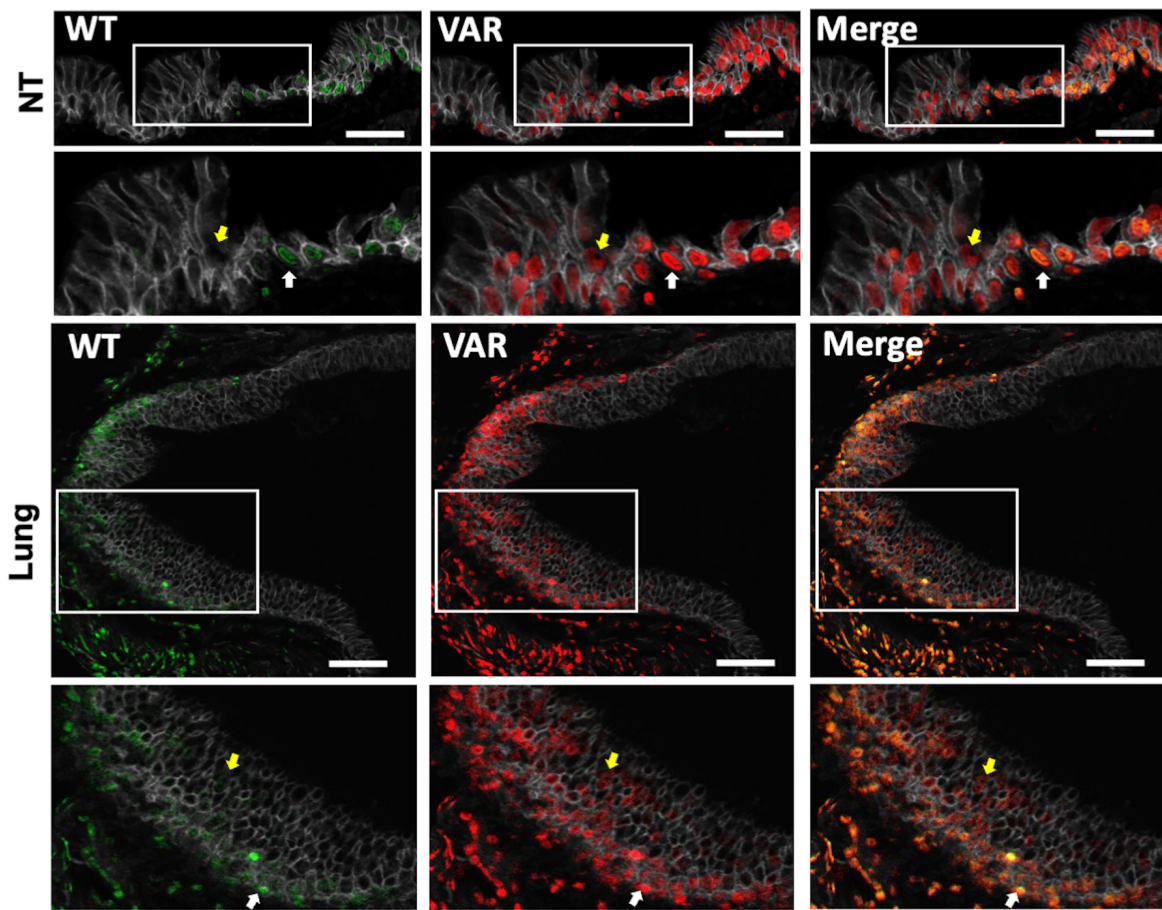
A



B



C



D

